Journal of Environmental Chemical Engineering 11 (2023) 110180

Contents lists available at ScienceDirect

Journal of Environmental Chemical Engineering

journal homepage: www.elsevier.com/locate/jece

Phosphorous recovery from water via batch adsorption enrichment combined with struvite crystallization in a fluidized bed reactor

Amadu T. Bah [1], Ziyi Shen [1], Junna Yan, Feihu Li [*,2]

Collaborative Innovation Center of Atmospheric Environment and Equipment Technology, Jiangsu Key Laboratory of Atmospheric Environment Monitoring and Pollution Control, School of Environmental Science and Engineering, Nanjing University of Information Science and Technology, 219 Ningliu Road, Nanjing 210044, China

ARTICLE INFO

Editor: Teik Thye Lim

Keywords:
Layered double hydroxides
P-preferring element
Anion exchange
Surface complexation
Recyclability

ABSTRACT

To assess the feasibility of recovering P from water by combining batch adsorption enrichment with struvite crystallization, we prepared four ternary layered double hydroxides (LDHs) with P-preferring elements (i.e., zirconium (Zr) or lanthanum (La)) via a facile coprecipitation method, and evaluated their performance in recovering P from water, particularly in enriching P from a low-level P solution. We find that all ternary LDHs demonstrate remarkably high P adsorption capacities, e.g., 1029.3 mg PO_4^{3-} g^{-1} for ZnAlLa, outperforming other LDHs reported so far. Microstructural analyses show that the P uptake mechanisms are attributable to anion exchange, surface complexation and electrostatic attraction. Results of recycling tests indicate that all LDHs present good enrichment for P. Besides, more than 96% of phosphorus in the P-enriched eluates can be efficiently reclaimed via struvite crystallization in a fluidized bed reactor. These findings demonstrate the feasibility of combining adsorption enrichment with struvite crystallization for P recovery.

1. Introduction

Phosphorus (P) is a crucial element for life on the earth, and particularly one of the three essential macronutrients for higher plants' growth and development. Due to unsustainable resource exploitation, excessive application of phosphate fertilizers in croplands and inadequate management of the human phosphorus cycle [9], humankind is facing two twinned problems: a diminishing supply of phosphate (i.e., 'rock phosphate') as a resource and an excess of phosphate (i.e., 'dissolved phosphate') in surface water streams causing eutrophication, which in turn degrades surface water quality [29,55]. Hence, removing and recovering P from various waste streams and converting it into P-containing products has been recognized as one of the most promising strategies to address both of the above issues simultaneously [12,34,44,46]. Indeed, numerous P recovery technologies have been developed successively, such as chemical precipitation, enhanced biological phosphorus removal (EBPR), crystallization, adsorption, etc. [15,48] In particular, some of these technologies have been practically implemented at a high industrial scale [15].

Of various P-recovery technologies from wastewater, adsorption has been gaining considerable attention due to its effectiveness, reliability, and environmental benignity [32,40,60]. In particular, adsorption is suitable for capturing phosphorus from low-P wastewaters, thus facilitating the subsequent efficient recovery of the captured phosphorus from the P-enriched eluates (i.e., the desorption matrix), which other technologies cannot achieve [20]. A great number of adsorbents have already been documented and comprehensively evaluated for their P recovery performance [3,36,60]. Of these, layered double hydroxides (LDHs) are extensively studied due to their characteristics of ideal adsorbents such as high adsorption capacity, fast adsorption rate, easy regeneration, and high stability [1,21,42,64]. Cheng et al. reported that calcinated ZnAl-LDHs can efficiently recover P from sludge filtrate by adsorption [6]. A recent study shows that ultrathin MgAl-LDHs nanoparticles adsorb up to ~ 55% more P than conventional MgAl-LDHs [38], but this will raise new challenges in recycling these P-loaded LDH nanoparticles. To prevent the loss of P-loaded adsorbent during the recycling process, such LDHs are usually either bound to porous carriers [33,49] or assembled with magnetic particles [35,37,41]. In general, P adsorption on LDHs is often subjected to competition from various co-occurring anions, e.g., nitrate, sulfate, chloride, and bicarbonate ions [42,52]. Interestingly, incorporation of a certain P-preferring element (e.g., La, Zr) into conventional LDHs can effectively enhance their P

* Corresponding author.
E-mail address: fhli@nuist.edu.cn (F. Li).
[1] These authors contributed equally to this work.
[2] https://orcid.org/0000-0002-2969-8276.

https://doi.org/10.1016/j.jece.2023.110180
Received 11 March 2023; Received in revised form 16 May 2023; Accepted 21 May 2023
Available online 23 May 2023

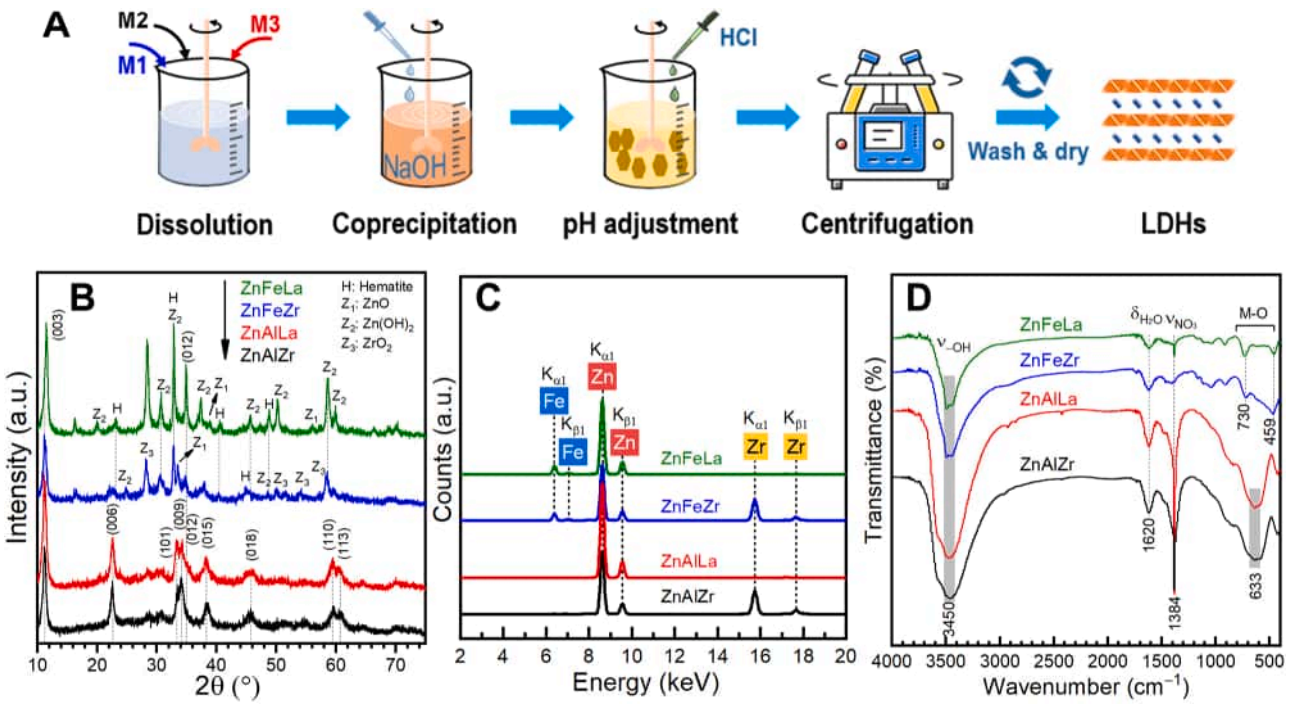

Fig. 1. (**A**) Schematical illustration of preparation of ternary LDHs (M1 −3 refer to different types of metal precursors); (**B**–**D**) Characterizations of the as-prepared ternary LDHs: (**B**) XRD patterns, (**C**) XRF, and (**D**) FT-IR spectra.

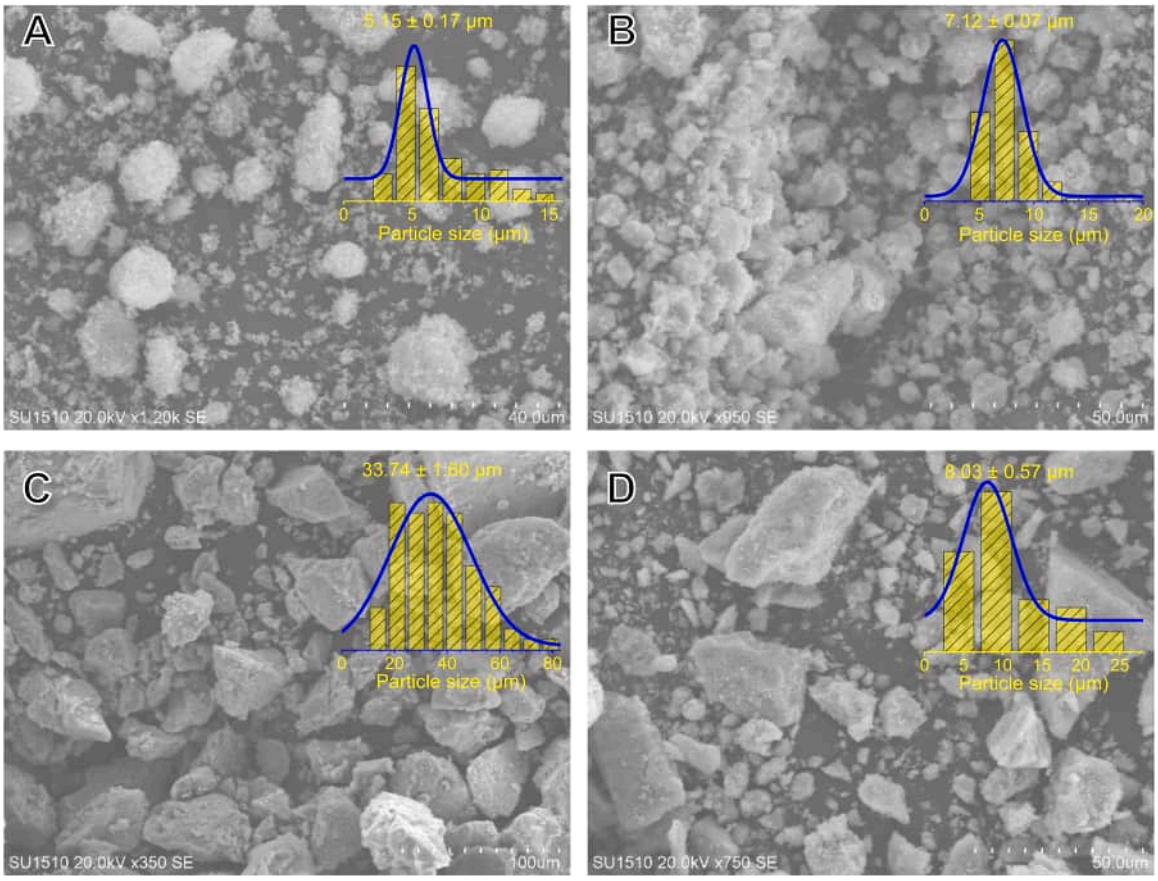

Fig. 2. SEM images of (**A**) ZnFeLa, (**B**) ZnFeZr, (**C**) ZnAlLa, and (**D**) ZnAlZr. Note: the inset is a histogram of the particle size distribution corresponding to each image.

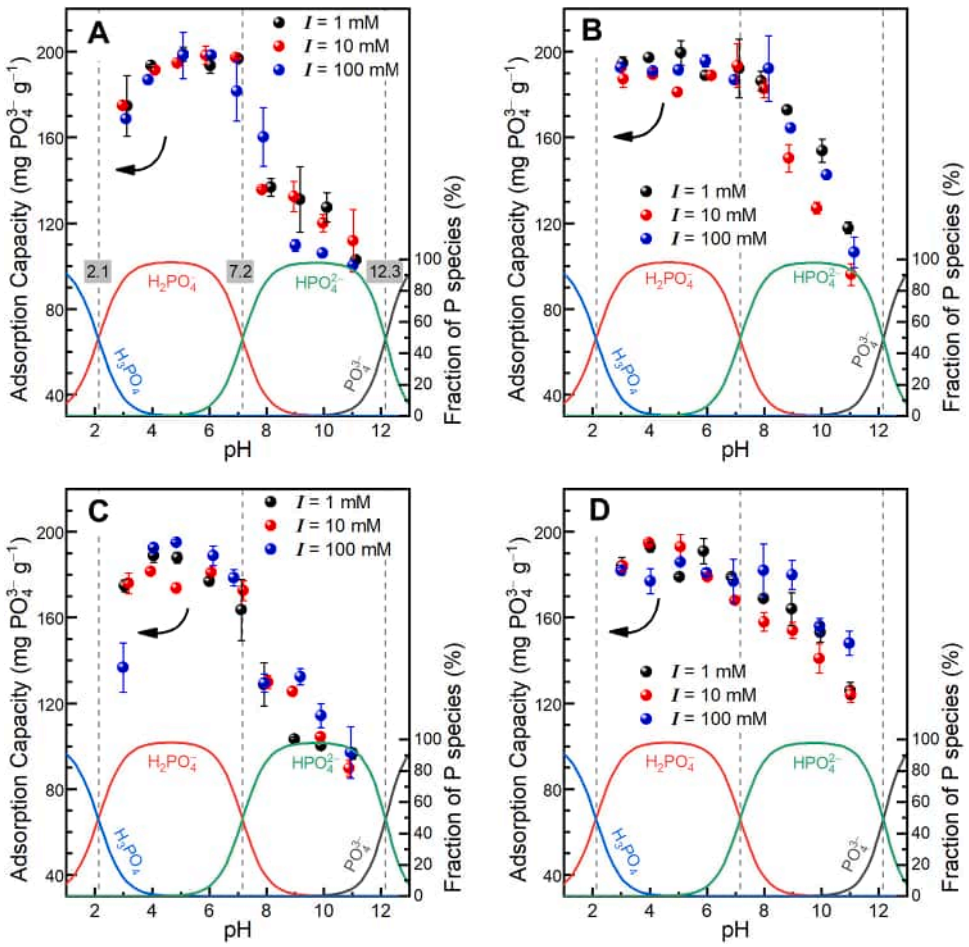

Fig. 3. Effects of pH and ionic strength on phosphate adsorption on (**A**) ZnFeLa, (**B**) ZnFeZr, (**C**) ZnAlLa, and (**D**) ZnAlZr. Note: the speciation diagram of 7.35×10^{-4} mol L^{-1} KH_2PO_4 solution at 25 °C is also included in each panel.

adsorption capacity and selectivity [30,32,37,67]. For instance, Drenkova-Tuhtan and co-workers thoroughly screened and evaluated a large group of ternary LDHs materials with different cation building blocks of such P-preferring elements [19,56], and assembled magnetic microparticles and LDHs into reusable adsorbents that have been implemented at a pilot scale [18,43].

As mentioned above, P recovery from waste streams aims at obtaining P-enriched products, usually in the form of solid precipitates that can be easily reused as feedstock in agriculture or industry, such as struvite, calcium phosphate, etc. [12,29] A recent report shows that struvite crystallization rather than desorption occurred when using ammonia solution as eluent for desorbing P from LDH adsorbent, and that the ammonia-treated P-loaded LDHs demonstrates improved P bioavailability in comparison to those of P-loaded LDHs, and pure struvite [62]. Undoubtedly, the P-loaded LDHs can be used directly as P-enriched products, e.g., slow-release fertilizers [16,21,31], but the cost-effectiveness of such a once-and-done strategy may be very high in comparison to a repeated-use scenario of LDHs adsorbents, and therefore needs to be reevaluated carefully. Despite many literature reporting the use of LDHs as adsorbents in the recovery of phosphorus from wastewater [22], however, there are few further in-depth studies on the subsequent treatment of P-enriched eluates (i.e., the liquors from P desorption). Struvite crystallization in a fluidized bed platform has been recognized as a highly efficient, scalable and reliable protocol for gaining solid P-containing products directly from nutrient-rich streams [5,27,34]. However, no study has been reported so far on the integration of adsorption/desorption enrichment using ternary LDHs with struvite crystallization in a fluidized bed for high-efficient P recovery from low-P effluents.

Inspired by the aforementioned studies, we herein systematically compared the adsorption/desorption enrichment performance of four promising ternary LDHs and then combined them with struvite crystallization in a fluidized bed for P recovery. First, four ternary LDHs with P-preferring elements were synthesized and systematically evaluated for their structural properties and P adsorption behaviors. Next, the P-enriched eluates from the desorption of P-loaded LDHs were fed into a fluidized bed reactor (FBR) along with other feedstocks for recovering P via struvite crystallization. The effect of the molar ratio of different feed sources on struvite quality was also investigated. This strategy of combining adsorption enrichment with crystallization is expected to be extended to the recovery of other valuable elements from waste streams.

2. Materials and methods

2.1. Chemicals

Iron (III) chloride hexahydrate ($FeCl_3 \cdot 6\ H_2O$, ≥ 97.0%), zirconium (IV) oxychloride octahydrate ($ZrOCl_2 \cdot 8\ H_2O$, 99.9%), zinc chloride ($ZnCl_2$, ≥ 98.0%), lanthanum nitrate hexahydrate ($La(NO_3)_3 \cdot 6\ H_2O$, 99.0%), aluminum nitrate nonahydrate ($Al(NO_3)_3 \cdot 9\ H_2O$, ≥ 98.0%) were purchased from Sinopharm Chemical Reagent Co., Ltd. (Shanghai, China) and used without further purification. All chemicals are of analytical grade or above unless otherwise specified. The stock solution of phosphorus (2000 mg L^{-1}) was prepared by dissolving 0.286 g of potassium dihydrogen phosphate (KH_2PO_4, 99.99%, Merck KGaA, Shanghai) in 100 mL of Milli-Q deionized water (18 MΩ-cm at 25 °C).

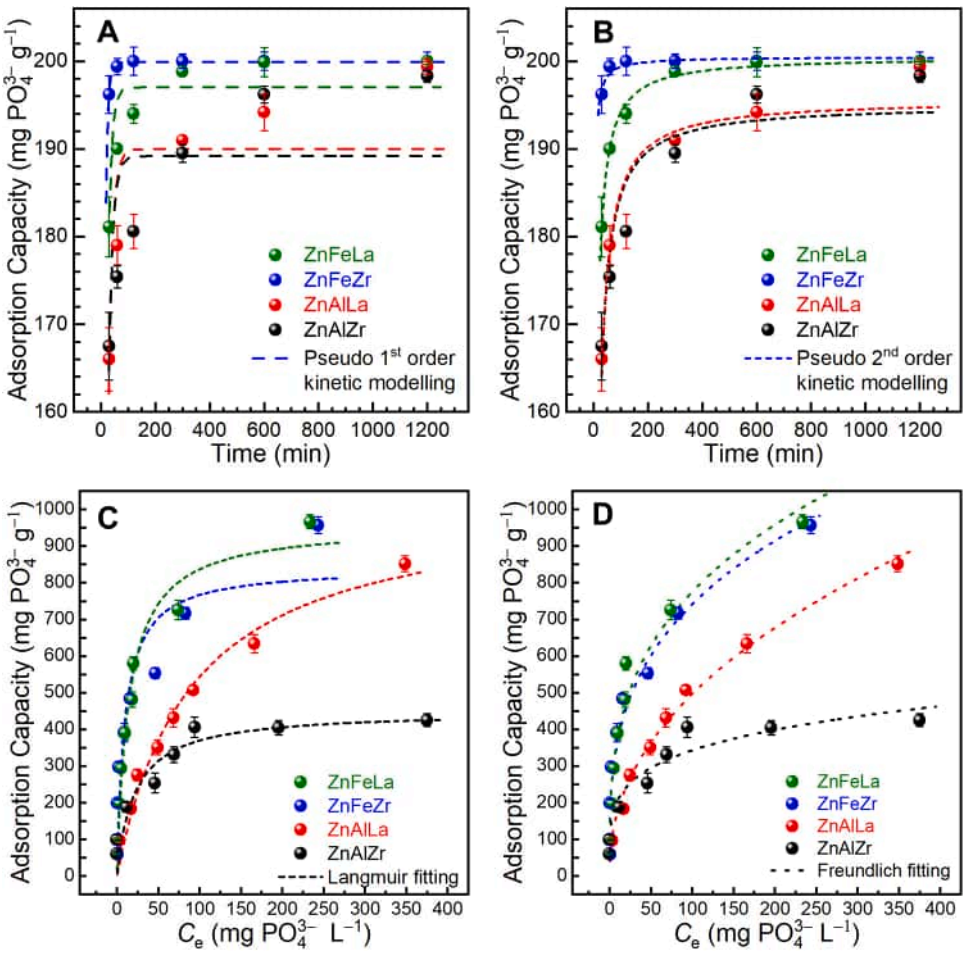

Fig. 4. Adsorption plots of phosphate on the four ternary LDHs: (**A**) adsorption kinetics with the Pseudo-first-order kinetic fitting plot, (**B**) adsorption kinetics with the Pseudo second-order kinetic fitting plot (adsorbent dosage =1 g L^{-1}, initial PO_4^{3-} = 200 mg L^{-1}, pH = 5, T = 25 °C), (**C**) adsorption isotherms with the Langmuir fitting plots, and (**D**) adsorption isotherms with the Freundlich fitting plots (adsorbent dosage =1 g L^{-1}, pH = 5, T = 25 °C).

The pH of all solutions was adjusted using NaOH or HNO_3 solutions.

2.2. Preparation of the ternary LDHs

By using a facile coprecipitation method based on a well-defined procedure [19], four ternary LDHs were synthesized with a constant M_1:M_2:M_3 precursor ratio of 6:1:1 (M_1 = Zn precursor; M_2 = Fe or Al precursor, M_3 = La or Zr precursor, see Fig. 1A). In brief, 8.18 g (0.06 mol) of $ZnCl_2$, 2.70 g (0.01 mol) of $FeCl_3{\cdot}6\ H_2O$ and 4.33 g (0.01 mol) of $La(NO_3)_3{\cdot}6\ H_2O$ were dissolved in 100 mL deionized water. The obtained precursor solution was added dropwise to 400 mL of 0.15 M NaOH solution under stirring (300 rpm) within 10 min. The resulting turbid suspension was then stirred for 5 min, followed by adjusting its pH to 7 with hydrochloric acid. Next, the solid sample (denoted as ZnFeLa) was centrifuged, washed twice with deionized water, and freeze-dried for further use. By using the same procedure with different metal precursors, three other LDHs were also prepared and denoted as ZnFeZr, ZnAlLa, and ZnAlZr, respectively.

2.3. Characterization

Powder X-ray diffraction (XRD) analysis of the samples was conducted on an XRD-6100 diffractometer (Shimadzu, Japan) at a tube voltage of 40 kV and a tube current of 30 mA with Cu-Kα radiation (step size: 0.02°, scanning rate: 5 ° min^{-1}). The morphological characteristics of all samples were obtained by a SU1510 scanning electron microscope (SEM, Hitachi, Japan) at an accelerating voltage of 1.5 kV. X-ray fluorescence spectroscopy (XRF) analysis was conducted on a handheld DELTA DC 4000 analyzer (Olympus, USA) with the soil mode. Fourier transform infrared spectroscopy (FT-IR) data were collected on an Is5 infrared spectrometer (Thermo Nicolet, USA). A PHI-5000 Versa Probe X-ray photoelectron spectrometer (XPS, UIVAC-PHI, Japan) employing a monochromatized Al Kα radiation (hν = 1486.6 eV) was used to probe the surface properties of the samples. The adventitious C 1 *s* peak (284.8 eV) was used for calibrating the binding energy.

2.4. Batch adsorption and desorption experiments

All batch adsorption and desorption experiments were performed in triplicate at room temperature (T, ca. 25 °C). For the effects of pH and ionic strength (I) experiments, the adsorption slurries were prepared in 10 mL polyethylene vessels by mixing 0.01 g adsorbents with a certain amount of phosphate stock solution and the background electrolyte solution, i.e., $NaNO_3$ (I = 1 mM, 10 mM, and 100 mM). The pH was then adjusted to 3 − 12 with diluted HNO_3 or NaOH solution, yielding a suspension with a constant adsorbent dose of 1 g L^{-1} and an initial phosphate (PO_4^{3-}, denoted as P) concentration of 20 mg L^{-1}. After rotating for 24 h on a Labquake tube rotator mixer (Thermo Scientific, USA) at 60 rpm, the suspensions were centrifuged at 8000 rpm for 15 min followed by filtrating with 45 μm mixed cellulose esters (MCE) membrane (Navigator, Tianjin) to reclaim the supernatants. The P concentration in the supernatants was determined by a UV–vis spectrophotometer (UV-9200, Beijing Rayleigh Instrument Co., China) at 700 nm following the standard ascorbic acid method as described

Table 1
Comparison of the theoretical adsorption capacities of various La/Zr-modified LDHs calculated by the Langmuir equation for phosphate removal.

Adsorbent	Experimental conditions (pH, *T*, dosage, initial/maximum content)	Type of wastewater	Q_m (mg PO_4^{3-} g^{-1})	Reference
3Mg(AlZr)-LDH (CO_3)	8.7, 25 °C, 1.0 g L^{-1}, 2 mg P L^{-1}	model wastewater	91.9	[8]
ZnAlZr4-HT	5.5, 30 °C, 1.0 g L^{-1}, 250 mg P L^{-1}	synthetic solution	303.4	[30]
MgFeZr-LDH@Fe_3O_4	4.5, 20 °C, 1.0 g L^{-1}, 10 mg P L^{-1}	effluent wastewater	107.3	[17]
ZnFeZr-LDH@Fe_3O_4	7.0, 24 °C, 1.0 g L^{-1}, 10 mg P L^{-1}	effluent wastewater	589.3	[18]
Fe_3O_4 @MgAl-LDH@La(OH)$_3$	7.0, 25 °C, 0.1 g L^{-1}, 12 mg P L^{-1}	synthetic solution	203.8	[37]
La-loaded MgFe-LDH	7.0, 25 °C, 0.5 g L^{-1}, 60 mg P L^{-1}	synthetic solution	33.4	[67]
ZnAlFeLa-LDH@Fe_3O_4	4.0, 30 °C, 1.2 g L^{-1}, 400 mg PO_4^{3-} L^{-1}	synthetic solution	165.9	[53]
ZnAlLa LDH	5.0, 25 °C, 1.0 g L^{-1}, 500 mg PO_4^{3-} L^{-1}	synthetic solution	1029.3	This study
ZnAlZr LDH	5.0, 25 °C, 1.0 g L^{-1}, 500 mg PO_4^{3-} L^{-1}	synthetic solution	499.6	This study
ZnFeLa LDH	5.0, 25 °C, 1.0 g L^{-1}, 500 mg PO_4^{3-} L^{-1}	synthetic solution	958.8	This study
ZnFeZr LDH	5.0, 25 °C, 1.0 g L^{-1}, 500 mg PO_4^{3-} L^{-1}	synthetic solution	842.2	This study

previously [36].

Likewise, the adsorption kinetics experiments were carried out with an initial P concentration of 200 mg L^{-1} and the same adsorbent dose of 1 g L^{-1} at pH 5.0, where P adsorption was most efficient over the four ternary LDHs and the monovalent the dihydrogen phosphate ions were the dominant P species (see Fig. 3). At different time intervals, the adsorption reaction was terminated, and three vessels were unmounted for supernatant sampling. The adsorption isotherms tests were also performed with increasing initial P concentrations from 10 to 500 mg L^{-1} (pH = 5.0). All the suspensions were rotated for 24 h to ensure the attainment of an equilibrium state. Subsequent centrifugation and filtration were also conducted, followed by measuring the P concentration in the supernatants. The P adsorption kinetic data were analyzed using both the Pseudo-first order (Eq. (1)) and the Pseudo-second order (Eq. (2)) kinetic models, whereas the adsorption isotherm data were fitted by the Langmuir (Eq. (3)) and the Freundlich (Eq. (4)) models. All the models are formulated as follows,

$$\frac{\ln(Q_e - Q_t)}{Q_e} = -k_1 t \tag{1}$$

$$\frac{t}{Q_t} = \frac{1}{k_2 Q_e^{\,2}} + \frac{t}{Q_e} \tag{2}$$

$$Q_e = \frac{k_L Q_m C_e}{1 + k_L C_e} \tag{3}$$

$$Q_e = k_F C_e^{1/n} \tag{4}$$

where $\boldsymbol{Q}_e$ and $\boldsymbol{Q}_t$ are the P adsorption capacity at equilibrium and at time t (mg PO_4^{3-} g^{-1}), respectively; $\boldsymbol{k}_1$ is the Pseudo-first order rate constant (min^{-1}); $\boldsymbol{k}_2$ is the Pseudo-second order rate constant (g mg^{-1} min^{-1}); $\boldsymbol{Q}_m$ is the theoretical maximum adsorption capacity (mg PO_4^{3-} g^{-1}), $\boldsymbol{C}_e$ is the concentration of the target adsorbate at equilibrium (mg L^{-1}), $\boldsymbol{k}_L$ is the Langmuir constant related to the free energy of adsorption (L mg^{-1}), $\boldsymbol{k}_F$ (mg^{1-n} L^n g^{-1}) and n are empirical constants of the Freundlich model.

By using a mixture of NaOH and Na_2CO_3 solution (1.0 M:1.0 M, pH = 13) as the desorbing eluent [19], desorption tests were conducted with an adsorbent dose of 10.0 g L^{-1} in 50 mL of the above eluent solution within 3 h. Based on kinetic experiments, a contact time of 3 h can enable adsorption efficiency as high as > 95% for all four ternary LDHs, and therefore was adopted in the recycling performance tests. With respect to recycling tests, a sequential adsorption-desorption test was performed in a consecutive manner of 3-h adsorption (adsorbent dose = 1.0 g L^{-1}, 500 mL of P-containing solution, initial PO_4^{3-} = 20 mg L^{-1}, pH = 5, 25 °C) followed by 3-h desorption (adsorbent dose = 10.0 g L^{-1}, 50 mL of eluent solution, pH = 13, 25 °C). Briefly, the spent adsorbents were recovered by centrifuging at 8 000 rpm, followed by solid-liquid separation in a handily pouring manner. The supernatant was then filtered through a 45 μm membrane for P analysis, while the spent adsorbents sticked to tube bottom were resuspended by adding a certain volume of the desorption matrix and rotated at 60 rpm for 3 h. Afterwards, the regenerated adsorbents were recovered in the same manner and further used for the next batch adsorption cycle. The P-containing solution is prepared to simulate the sludge dewatering liquid of a local sewage treatment plant with PO_4^{3-} concentration in the range of 15 – 40 mg L^{-1}. To obtain a P-enriched eluate, a fresh P solution was used in each adsorption test, whereas the same eluent (i.e., 50 mL of NaOH--Na_2CO_3 mixture) was repeatedly employed in the desorption operations. The phosphate concentration in supernatants and/or eluates from each adsorption/desorption cycle were measured accordingly.

2.5. Struvite crystallization in a fluidized-bed reactor

To further reclaim P from eluates of the desorption experiments, struvite crystallization experiments were performed in a homemade FBR ($\boldsymbol{\Phi}$ = 4 cm, $\boldsymbol{l}$ = 36 cm) as shown in Fig. S1 (Supplementary materials). The P-enriched eluates were collected and analyzed. Then, the solution pH was adjusted to about 11, because a drop in pH value to 9 − 9.5 was often observed, which is the optimal pH value for struvite precipitation [39]. Next, the P solution along with the magnesium source (2.0 mM, solution prepared with $MgCl_2{\cdot}6\ H_2O$), ammonium source (2.0 mM, solution prepared with NH_4Cl), were fed into the FBR by three peristaltic pumps (BT-100, Longer Pump Co., China) at varying feed rates. The fourth pump linking the bottom and the upper top of the reactor was used to circulate the mixture for attaining a fluidization state. The effect of the molar ratio of Mg^{2+}:NH_4^+:PO_4^{3-} (denoted as Mg:N:P ratio) on the property of synthetic struvite was also explored by regulating the flow rate of the above peristaltic pumps.

The struvite crystals were harvested from the bottom of the reactor after the feed, and recycle feed flows were terminated within 30 min, and the crystals were allowed to settle down and deposited in a conical settling tank, from which they are subsequently separated and reclaimed. The harvested struvite crystals were then washed with deionized water for three times, followed by air drying for 12 h before further characterizations.

3. Results and discussions

3.1. Characterization of the ternary LDHs

The XRD patterns of ZnFeZr, ZnFeLa, ZnAlLa and ZnAlZr are shown in Fig. 1B. The patterns of both Al-containing LDHs, i.e., ZnAlLa and ZnAlZr, exhibit a group of well-defined reflections such as (003), (006), (009), (015), etc., which are assignable to the characteristic peaks of conventional LDHs [19,28]. In the case of Fe-bearing LDHs, however,

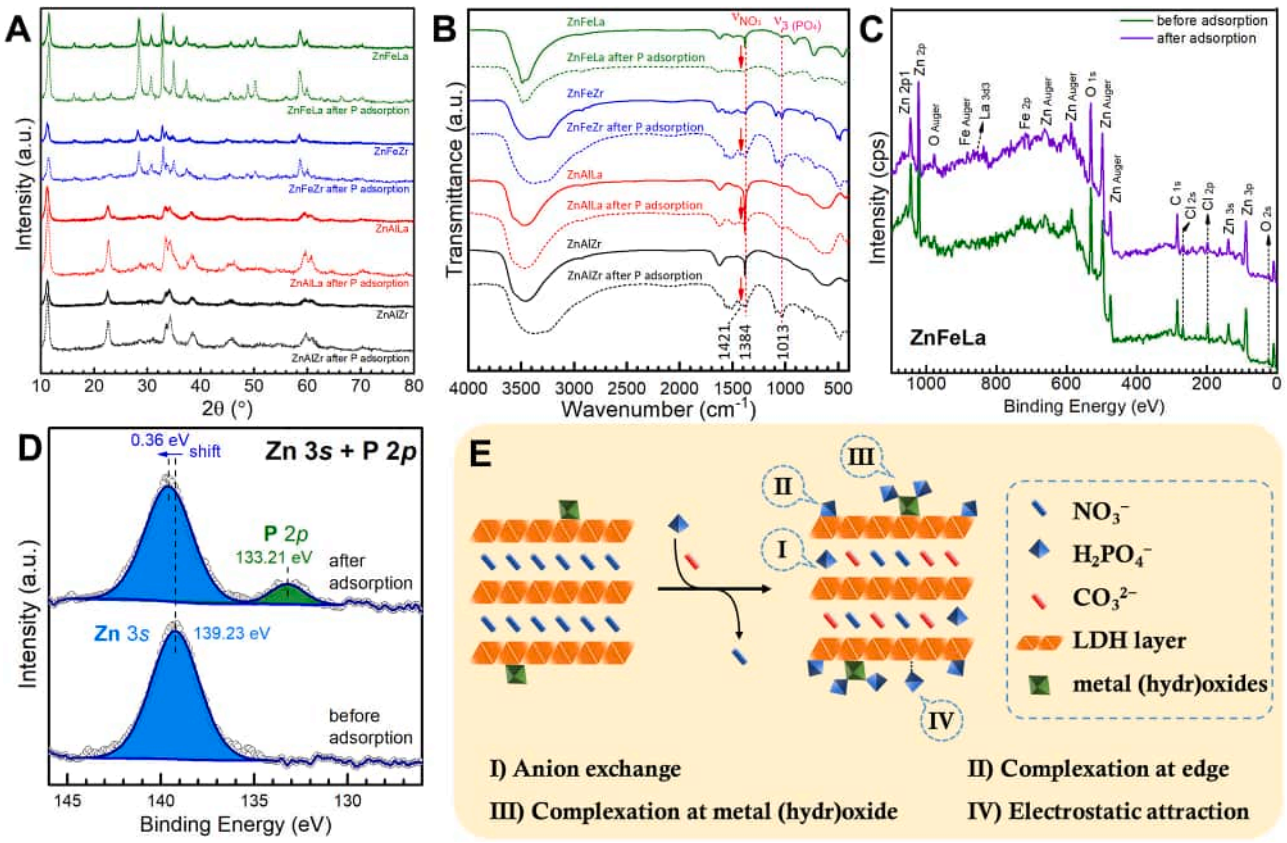

Fig. 5. Microscopic structure comparison of the ternary LDHs before and after P adsorption: (**A**) XRD patterns, (**B**) FT-IR spectra, (**C**) XPS survey spectra of ZnFeLa, and (**D**) Zn 3 s and P 2p XPS regions of ZnFeLa, (**E**) Proposed adsorption mechanism for P uptake on the ternary LDHs.

their patterns show various additional reflections besides those of typical LDHs with the same miller indices as both ZnAlLa and ZnAlZr. These reflections are sharp, and along with a low and stable baseline, suggesting that the samples are well-crystallized. Besides, these reflections match well with standard XRD patterns of zinc oxide (ZnO, JCPDS #65–2880, labeled with Z_1), sweetite ($Zn(OH)_2$, JCPDS #38–0356, labeled with Z_2), iron oxide (Fe_2O_3, JCPDS #39–0238, labeled with H), and zirconia (ZrO_2, JCPDS #89–9066, labeled with Z_3), respectively [19,54]. As the position of the basal reflection (003) usually depends on the distance between two adjacent metal hydroxide sheets in LDHs [59], the *d* spacing of (003) reflection was calculated to be 7.66, 7.87, 7.86, and 7.88 Å for ZnFeLa, ZnFeZr, ZnAlLa, and ZnAlZr, respectively. All of these *d* spacing values far outstrip the size of phosphate ion (4.76 Å) [8], offering channels wide enough for the diffusion and migration of P.

XRF analyses of four ternary LDHs confirm the existence of major elements, i.e., Fe, Zn, Zr, etc. (Fig. 1C). Note that no peaks for the principal K-shell lines of both Al and La element were observed in the relevant XRF spectra, because both elements are undetectable or below the limits of detection of the handheld XRF analyzer especially in the soil mode [51]. The FT-IR spectra of all ternary LDHs are presented in Fig. 1D. The hydroxyl vibrational band at 3474 cm^{-1} and the intense band at 1617 cm^{-1} are attributable to O-H stretching and H-O-H bending vibration of the adsorbed water molecules, respectively [56]. The band at 1382 cm^{-1} refers to the antisymmetric stretching vibration of nitrate (NO_3^-) intercalated in the interlayer space [28]. It is worth noting that no IR band assignable to chloride (Cl^-) was observed even though both nitrate and chloride salts were employed as parent materials. This can be well explained by the fact that nitrate is more preferentially intercalated into LDHs than chloride ions [7]. Besides, a series of bands is present in the range of 800–400 cm^{-1}, which are attributed to M-O stretching or M-O-M bending vibrations (i.e., M = Zn, Al, La, Fe and Zr) [30,33,56]. The morphology of four ternary LDHs is characterized by irregular grit-shaped particulates with average sizes of 5.15, 7.12, 33.74, and 8.03 μm for ZnFeLa, ZnFeZr, ZnAlLa, and ZnAlZr, respectively (Fig. 2), which is comparable with other ternary LDHs reported elsewhere [17,18].

3.2. Effects of pH and ionic strength on phosphate adsorption

The effect of solution pH is a regular paradigm for adsorption studies since pH not only affects the speciation of adsorbate but also has a defining impact on the surface charge of the adsorbent [23]. As shown in Fig. 3, P adsorption on all ternary LDHs is pH-dependent and ***I***-independent. It is obvious that P adsorption increases and then decreases slightly as the solution pH increases from 2 to 7, attaining a maximum at pH ~ 5, where nearly all P is present as $H_2PO_4^-$. This observation is in good agreement with previous reports [52], and indicates that the anion exchange reaction between P from bulk solution and nitrate from ternary LDHs dominates at this stage [13,26]. This reaction can be further verified by the FT-IR spectra in the following section. As pH continually increases beyond 7.2 (pK_{a2} of phosphate), P adsorption proceeds to decrease rapidly. Because the ternary LDHs are likely to be negatively charged due to the surface enrichment of free hydroxyl ions at a higher pH [28], and the dominant P species turns from negative monovalent $H_2PO_4^-$ to negative divalent HPO_4^{2-}, and even trivalent PO_4^{3-} as pH increases beyond 7.2, it is therefore not surprising to observe the sharp decrease in P adsorption due to the strong electrostatic repulsion between the negatively charged LDHs and the higher negative P species. Nevertheless, the optimal pH favoring P adsorption was selected to be 5 with respect to the maximum adsorption capacities for all ternary LDHs.

In addition, ions exhibiting little or no ionic strength dependence of adsorption were considered to form strong inner-sphere surface complexes; ions showing significant ionic strength dependence were

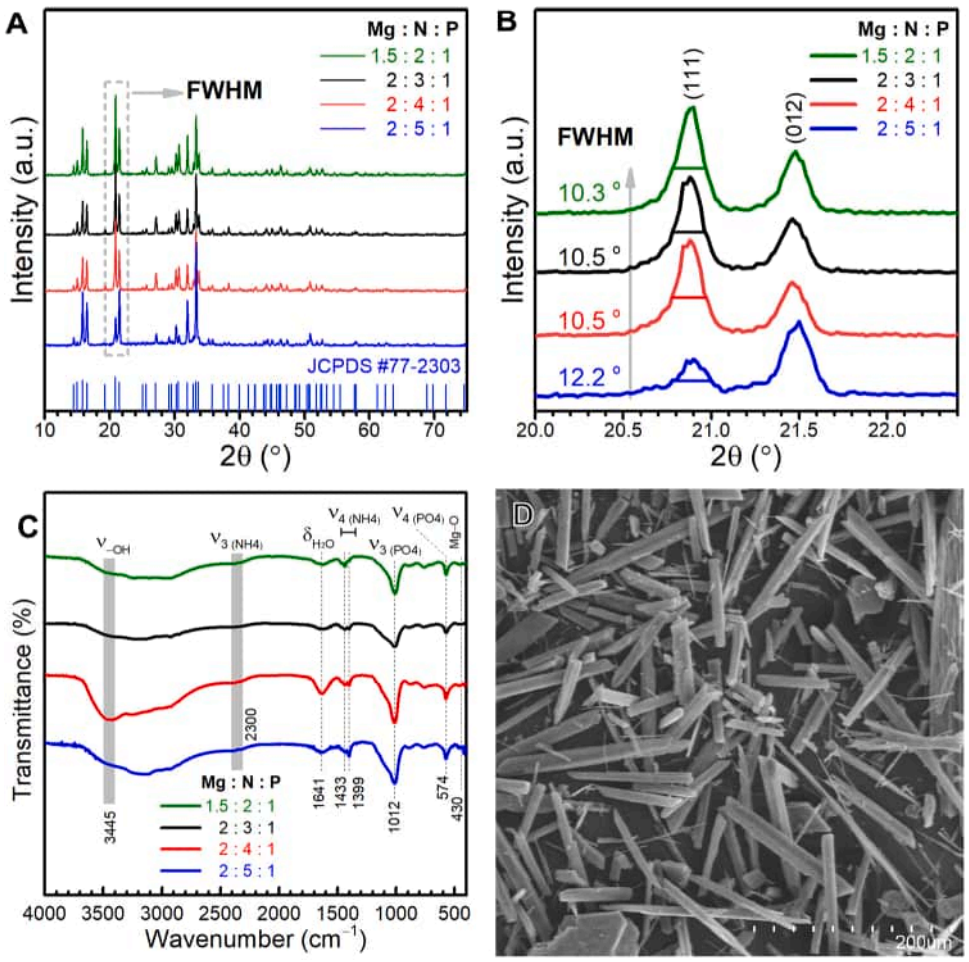

Fig. 6. Characterization of the reclaimed struvite derived from systems with varying Mg:N:P ratios: (**A**) XRD patterns, (**B**) Comparison of the FWHM data of the (111) reflections in the XRD patterns, (**C**) FT-IR spectra, and (**D**) SEM image of the struvite with an Mg:N:P ratio of 2:4:1.

supposed to be weakly adsorbed as outer-sphere surface complexes [45]. However, we cannot simply attribute inner-sphere surface complexation to the main adsorption mechanism responsible for P uptake since conventional LDHs often show a higher preference for P over nitrate [7,47]. Nonetheless, although anion exchange is usually recognized as the principal adsorption mechanism of LDHs adsorbents [13,62], there is also much spectroscopic evidence suggesting that surface complexation at the edges of LDHs can also play a significant contribution to P adsorption [38,47,67].

3.3. Adsorption kinetics

Adsorption kinetic data and the fitting curves of P on four ternary LDHs are depicted in Fig. 4 A and 4B. As observed, P ions were rapidly adsorbed within the initial 1 h, achieving up to 99.7%, 95.0%, 89.8%, and 88.5% of the calculated maximum adsorption capacity by the end of 1 h for ZnFeZr, ZnFeLa, ZnAlLa and ZnAlZr, respectively. It is interesting to notice that the adsorption equilibrium state of P on ZnFeZr and ZnFeLa was attained at 2 h and 6 h, respectively, whereas both ZnAlLa and ZnAlZr, composed of pure LDHs phase, required 20 h at least to achieve an adsorption equilibrium (Fig. 4 A), which is also comparable to the data in previous studies [17,64]. This observation suggests that P adsorption on both ZnAlLa and ZnAlZr is likely to be governed by the diffusion of P into the LDHs interlayers and the subsequent anion exchange between P and the intercalated nitrate ions. For ZnFeZr and ZnFeLa, initial rapid adsorption on several co-occurring metal oxides/hydroxides (e.g., ZnO, $Zn(OH)_2$, Fe_2O_3, and ZrO_2) followed by anion exchange with the intercalated nitrate appears to be the actual adsorption processes occurring as inferred from the kinetic curves and the XRD data. This interpretation also well explains why ZnFeZr demonstrated the fastest adsorption rate with the smallest *d* spacing of (003) reflection (i.e., 7.66 Å) and many metal oxides/hydroxides, in particular the P-preferring zirconium dioxide [24,56].

The best-fit kinetic parameters and the corresponding correlation coefficients (R^2) were calculated using the nonlinear curve fit tool in Origin 9.0 (64-bit version, OriginLab Co.) and are tabulated in Table S1. The correlation coefficients calculated by the Pseudo-first order kinetic model (R^2 = 0.449 – 0.976) are lower than those from the Pseudo-second order model (R^2 = 0.862 – 0.991), indicating that the P adsorption on these ternary LDHs appears to follow the Pseudo-second order model. This implies that P adsorption on these ternary LDHs involves in chemisorption, which is most likely the rate-limiting step of the adsorption process [36,63]. Similar trends were also observed for P adsorption on LDHs with different elements [6,25,66]. Considering that P adsorption on the ternary LDHs, e.g., ZnAlLa and ZnAlZr, required 20 h at least to achieve an equilibrium state, subsequent adsorption experiments were performed with a constant period of 24 h.

3.4. Adsorption isotherms

Fig. 4C and 4D present the adsorption isotherm data and the fitting curves of P on the ternary LDHs. Both the Langmuir and the Freundlich models were employed for fitting the experimental data and the best-fit parameters calculated by Origin 9.0 are given in Table S2. According to

the change in slope of the isotherm curve, the P adsorption isotherms may be classified as an L-type isotherm [57], which is characterized by a decreasing slope as the adsorbate concentration increases. Such adsorption behavior was often observed for P adsorption on LDHs-type adsorbents [11,25,59], and could be explained by the high affinity of the adsorbent for the adsorbate. As shown in Table S2, the correlation coefficients calculated by the two models are relatively high ($R^2 = 0.816 – 0.991$) and comparable to each other, implying that both the Langmuir and the Freundlich models can highly match the experimental data of P on these ternary LDHs. In addition, we can note that all the *n* values, determined by the Freundlich equation, are greater than 1 (Table S2). This indicates that P adsorption on these ternary LDHs appears to be a favorable process [8,18].

The maximum adsorption capacities, defined by the Langmuir model, are 842.2, 958.8, 499.6 and 1029.3 mg PO_4^{3-} g^{-1} for ZnFeZr, ZnFeLa, ZnAlZr and ZnAlLa, respectively. Their adsorption maxima outperform those of other La/Zr-modified LDHs-type adsorbents reported so far for P removal (Table 1), such as ternary 3Mg(AlZr)- LDH (CO_3) [8], ZnAlZr4-HT [30], La-loaded MgFe-LDH [67], and quaternary ZnAlFeLa-LDH@Fe_3O_4 [53], and are comparable to that of ZnFeZr-LDH@Fe_3O_4 (589.3 mg PO_4^{3-} g^{-1}) [18]. Therefore, it can be expected that such a large adsorption capacity of LDHs towards P could highly facilitate the subsequent P enrichment.

3.5. Adsorption mechanisms

To explore the underlying mechanisms of P uptake, a portion of the ternary LDHs before and after P adsorption were collected and characterized microstructurally (Fig. 5A − 5D, and S2). As observed in Fig. 5A, all the (003) reflections shifted slightly to the left, i.e., higher *d* spacing value. Given the fact that the size of phosphate ion (4.76 Å) is greater than nitrate ion (3.58 Å), and that a complete exchange of the intercalated nitrate with P would lead to fundamental changes in the XRD pattern [21], the above observation of slight increasing *d* spacings thus indicates the partial occurrence of anion exchange between P and the nitrate ions intercalated in LDHs [21]. In addition, all reflections in XRD patterns remained and their intensities were enhanced to some extent after P adsorption, indicating that all ternary LDHs have high stability and that P adsorption could improve the crystallinity of LDHs somewhat as reported earlier for P adsorption on MgFe-LDHs [61]. Besides, the presence of P on the P-loaded LDHs can also be verified by their FT-IR spectra (Fig. 5B), which are characterized by the arising of a new band (1013 cm^{-1}) attributable to $\nu 3$ vibration (antisymmetric stretching) of phosphate [58], and the recession or disappearance of the nitrate band (1384 cm^{-1}) as compared to the pristine ones. This spectral evidence further demonstrates the exchange reaction between the phosphate in solution and the nitrate intercalated in the ternary LDHs. Note that a weak shoulder band (labeled with red arrows) at 1421 cm^{-1} assignable to $\nu 3$ vibration of carbonate [4] was also detected, suggesting that anion exchange between the intercalated nitrate and the carbonate from dissolved air is likely to occur along with P adsorption.

Moreover, XPS spectra of ZnFeLa also verify the capture of P by such LDHs (Figs. 5C, 5D). It is worth noting that all the Zn 3 s, Zn 2p, O 1 s, Fe 2p, and La 3d XPS regions shifted toward a higher energy direction slightly upon P adsorption (Fig. 5D and S2), indicating that all these elements are chemically involved in P adsorption [49,61]. Note that the energy difference of two peaks of the La $3d_{5/2}$ spin-orbit splitting component is 3.4 eV (Fig. S2D), implying the existence of trace $La_2(CO_3)_3$ compound in ZnFeLa. The O 1 s XPS regions deconvoluted by Thermo Avantage (version 5.979) demonstrate that the surface oxygen species in the pristine ZnFeLa is composed of metal carbonate (denoted as O^{2-}, 13.8%), metal hydroxide (denoted as OH^-, 81.3%) and water (H_2O, 4.9%) (Fig. S2A). After P adsorption, the percentage of metal hydroxide was increased by 8.8% due to the surface complexation of phosphate. Given the above microstructural evidence and analyses, we can therefore attribute the primary mechanism of P uptake to i) anion exchange between the intercalated nitrate and P, ii) surface complexation at the edge of LDHs, iii) surface complexation at the water/co-occurring metal (hydr)oxides interface due to ligand exchange reactions between the metal (hydr)oxides and the phosphate ions, and iv) electrostatic attraction by the positively charged surface of the adsorbents in particular at lower pH (Fig. 5E).

3.6. Desorption and recycling of P-loaded LDHs

It is one of the essential criteria for a given adsorbent to be easily reclaimed from the exhausted one with the aim of multiple reuses. Meanwhile, the adsorption-desorption cycling performance of a certain adsorbent is crucial for the enrichment and recovery of specific valuable elements from wastewater streams. A mixture of NaOH and Na_2CO_3 (1.0 M:1.0 M) was selected as the eluent given its relatively high desorption efficiency for releasing P from the exhausted ternary LDHs [19]. The sequential adsorption-desorption tests of four ternary LDHs were conducted for 5 cycles and the results are present in Fig. S3. Obviously, the adsorption efficiencies (defined as the percentage of P loaded on LDHs in each adsorption test cycle) of all ternary LDHs exhibit an identical degressive trend, decreasing by 24.1%, 29.7%, 28.0%, and 29.3% after 5 cycles for ZnFeZr, ZnFeLa, ZnAlZr and ZnAlLa, respectively. Likewise, the desorption efficiencies (defined as the ratio of the desorbed to the previously loaded P) also show a similar overall degressive pattern, even though there are occasional increases in efficiency in some desorption cycles (Figs. S3B, S3C). Such trends in adsorption and desorption efficiencies have been frequently observed for other LDHs-type adsorbents towards P uptake [6,17,50]. This might be attributed to the loss of active adsorption sites due to partial dissolution of surface metals or insufficient desorption of phosphate from specific sites during the sequential adsorption-desorption operations.

Moreover, P concentrations in the eluates after 5 adsorption-desorption cycles were determined to be 58.71, 61.04, 53.32, and 52.09 mg L^{-1} for ZnFeZr, ZnFeLa, ZnAlZr and ZnAlLa, respectively. The corresponding enrichment factors (defined as the ratio of P concentrations in the final eluate and the initial P-containing solution) are 2.9, 3.1, 2.7, and 2.6, respectively, which are comparable to the data reported earlier for other ternary LDHs [18]. It is expected that more cycles will be required to achieve a sufficient enrichment of P if a solution with lower levels of P is used. Given that a P concentration of ~ 60 mg L^{-1} is sufficient for recovery of P via struvite crystallization [14,34], and that more cycles would be time-consuming and increase operational costs, the recycling test was thus terminated after five cycles in the present study. Nevertheless, the potential drawbacks of using ternary LDHs as adsorbents for P recovery might the high operating costs in pilot-scale applications, which would be addressed in future research by immobilizing such ternary LDHs on porous matrix followed by column adsorption-desorption.

3.7. P recovery via struvite crystallization

Using the above P-enriched eluate from 5 adsorption-desorption cycles of ZnFeLa as the feed solution, P recovery tests via struvite crystallization in an FBR were conducted by employing magnesium chloride solution (2.0 mM) and ammonium chloride solution (2.0 mM) as the companion feeds. In general, an over-stoichiometric ratio of Mg:N:P rather than the theoretical ratio of 1:1:1 is favorable for improving P recovery efficiency [18]. Therefore, reaction systems with Mg:N:P ratios of 1.5:2:1, 2:3:1, 2:4:1, and 2:5:1 were evaluated with regard to their impact on the quality of the resultant struvite precipitate, and the results are shown in Fig. 6 and S4. Note that all the reflections in XRD patterns of the reclaimed precipitates with varying Mg:N:P ratios match well to that in the standard XRD pattern of struvite (JCPDS #77–2303) (Fig. 6A). This observation confirms that a high purity struvite was obtained for all reaction systems, which can also be verified by the FT-IR spectra (Fig. 6C) and the SEM images (Fig. 6D and S4), demonstrating a

set of fingerprint infrared bands attributable to struvite [58], and the characteristic rod-like morphology [18], respectively. Further comparison in the full width at half maximum (FWHM) data of the (111) reflection indicates that the precipitate from the system with an Mg:N:P ratio of 1.5:2:1 has the smallest FWHM value (i.e., 10.3°) (Fig. 6B), demonstrating the largest grain size among these precipitates [65].

Interestingly, an attempt using an Mg:N:P ratio of 2:2:1 yielded newberyite ($MgHPO_4{\cdot}3\ H_2O$, JCPDS #72–0023) rather than struvite, which has been confirmed by the corresponding XRD and FT-IR results (Fig. S5). Given the fact that newberyite appears mostly in the system with excess magnesium [2], it is, therefore, most likely to form newberyite in the system with the richest magnesium (i.e., Mg:N:P ratio = 2:2:1). The reclaimed newberyite is featured by a diverse morphology of irregular particles (Fig. S5C, D), completely different from the rod-like struvite. Moreover, the newberyite also shows a different color from struvite, buff versus white (Fig. S6). Nevertheless, the P-recovery efficiency, defined as the percent of P reclaimed as the precipitate, exceeded 90% for all systems of varying Mg:N:P ratios (Fig. S7), with the highest efficiency of 96.3% for the system with an Mg:N:P ratio of 2:5:1. This is very comparable to that obtained for the Mg:N:P ratio of 1.5:1.5:1 reported elsewhere [18]. Therefore, such high P recovery efficiency together with the high purity of reclaimed struvite demonstrate the feasibility of the proposed strategy of combining adsorption enrichment with struvite crystallization for P recovery. Nonetheless, real wastewaters (e.g., sludge dewatering liquids) are often rich in both P and ammonium, which can be simultaneously recovered by struvite crystallization in an FBR [10]. Further studies on enrichment of both P and ammonium from a real sludge dewatering liquid by the ternary LDHs, therefore, is necessary and indeed an ongoing project by our group to facilitate the application of this technology in a real-life scenario for P and ammonium recovery.

4. Conclusions

In summary, we propose and validate a P-recovery strategy of combining adsorption enrichment using ternary LDHs as adsorbents with struvite crystallization in a fluidized bed reactor employing the P-enriched eluates as feed streams. The ternary LDHs (i.e., ZnFeZr, ZnFeLa, ZnAlZr and ZnAlLa) are rich in P-preferring elements, i.e., Zr or La, leading to extremely high adsorption capacities towards P (e.g., 958.8 and 1029.3 $PO_4^{3-}\ g^{-1}$ for ternary ZnFeLa and ZnAlLa, respectively) compared to conventional LDHs materials. Adsorption-desorption cycling tests and microstructural characterizations show that the underlying mechanisms for P uptake by the four ternary LDHs are involved in anion exchange, surface complexation via ligand exchange reactions, as well as electrostatic attraction. The results of struvite crystallization tests indicate that a highly pure struvite can be obtained from reaction systems with varying Mg:N:P ratios except for the system with an Mg:N:P ratio of 2:2:1 yielding newberyite instead of struvite. Our findings advance the development of multielement LDHs adsorbents incorporated with P-preferring elements and provide important insights for future innovation of novel strategies for P recovery from waste streams.

CRediT authorship contribution statement

Amadu T. Bah: Investigation, Formal analysis, Visualization, Writing – original draft; **Ziyi Shen:** Investigation, Formal analysis, Data curation, Visualization, Writing – original draft. **Junna Yan:** Visualization, Investigation, Validation. **Feihu Li:** Conceptualization, Funding acquisition, Resources, Supervision, Visualization, Writing – review & editing.

Declaration of Competing Interest

The authors declare that they have no known competing financial interests or personal relationships that could have appeared to influence the work reported in this paper.

Data Availability

Data will be made available on request.

Acknowledgments

The work was partially supported by the National Natural Science Foundation of China (51002080, 51310105009).

Appendix A. Supporting information

Supplementary data associated with this article can be found in the online version at doi:10.1016/j.jece.2023.110180.

References

[1] S.M. Ashekuzzaman, J.Q. Jiang, Study on the sorption-desorption-regeneration performance of Ca-, Mg- and CaMg-based layered double hydroxides for removing phosphate from water, Chem. Eng. J. 246 (2014) 97–105, https://doi.org/10.1016/j.cej.2014.02.061.
[2] V. Babic-Ivancic, J. Kontrec, L. Brecevic, D. Kralj, Kinetics of struvite to newberyite transformation in the precipitation system MgCl2-NH4H2PO4-NaOH-H2O, Water Res 40 (18) (2006) 3447–3455, https://doi.org/10.1016/j.watres.2006.07.026.
[3] H. Bacelo, A.M.A. Pintor, S.C.R. Santos, R.A.R. Boaventura, C.M.S. Botelho, Performance and prospects of different adsorbents for phosphorus uptake and recovery from water, Chem. Eng. J. 381 (2020), 122566, https://doi.org/10.1016/j.cej.2019.122566.
[4] A. Bah, J. Jin, A.O. Ramos, Y. Bao, M.Y. Ma, F.H. Li, Arsenic(V) immobilization in fly ash and mine tailing-based geopolymers: performance and mechanism insight, Chemosphere 306 (2022), 135636, https://doi.org/10.1016/j.chemosphere.2022.135636.
[5] A. Britton, F.A. Koch, D.S. Mavinic, A. Adnan, W.K. Oldham, B. Udala, Pilot-scale struvite recovery from anaerobic digester supernatant at an enhanced biological phosphorus removal wastewater treatment plant, J. Environ. Eng. Sci. 4 (4) (2005) 265–277, https://doi.org/10.1139/S04-059.
[6] X. Cheng, X.R. Huang, X.Z. Wang, B.Q. Zhao, A.Y. Chen, D.Z. Sun, Phosphate adsorption from sewage sludge filtrate using zinc-aluminum layered double hydroxides, J. Hazard. Mater. 169 (1–3) (2009) 958–964, https://doi.org/10.1016/j.jhazmat.2009.04.052.
[7] R. Chitrakar, S. Tezuka, A. Sonoda, K. Sakane, K. Ooi, T. Hirotsu, Adsorption of phosphate from seawater on calcined MgMn-layered double hydroxides, J. Colloid Interface Sci. 290 (1) (2005) 45–51, https://doi.org/10.1016/j.jcis.2005.04.025.
[8] R. Chitrakar, S. Tezuka, A. Sonoda, K. Sakane, K. Ooi, T. Hirotsu, Synthesis and phosphate uptake behavior of Zr4+ incorporated MgAl-layered double hydroxides, J. Colloid Interface Sci. 313 (1) (2007) 53–63, https://doi.org/10.1016/j.jcis.2007.04.004.
[9] D. Cordell, J.O. Drangert, S. White, The story of phosphorus: global food security and food for thought, Glob. Environ. Change-Hum. Policy Dimens 19 (2) (2009) 292–305, https://doi.org/10.1016/j.gloenvcha.2008.10.009.
[10] P. Cornel, C. Schaum, Phosphorus recovery from wastewater: needs, technologies and costs, Water Sci. Technol. 59 (6) (2009) 1069–1076, https://doi.org/10.2166/wst.2009.045.
[11] J. Das, B.S. Patra, N. Baliarsingh, K.M. Parida, Adsorption of phosphate by layered double hydroxides in aqueous solutions, Appl. Clay Sci. 32 (3–4) (2006) 252–260, https://doi.org/10.1016/j.clay.2006.02.005.
[12] L.E. de-Bashan, Y. Bashan, Recent advances in removing phosphorus from wastewater and its future use as fertilizer (1997-2003), Water Res 38 (19) (2004) 4222–4246, https://doi.org/10.1016/j.watres.2004.07.014.
[13] L. Deng, Z. Shi, Synthesis and characterization of a novel Mg-Al hydrotalcite-loaded kaolin clay and its adsorption properties for phosphate in aqueous solution, J. Alloy. Compd. 637 (2015) 188–196, https://doi.org/10.1016/j.jallcom.2015.03.022.
[14] E. Desmidt, K. Ghyselbrecht, A. Monballiu, K. Rabaey, W. Verstraete, B. D. Meesschaert, Factors influencing urease driven struvite precipitation, Sep. Purif. Technol. 110 (2013) 150–157, https://doi.org/10.1016/j.seppur.2013.03.010.
[15] E. Desmidt, K. Ghyselbrecht, Y. Zhang, L. Pinoy, B. Van der Bruggen, W. Verstraete, K. Rabaey, B. Meesschaert, Global phosphorus scarcity and full-scale P-recovery techniques: a review, Crit. Rev. Environ. Sci. Technol. 45 (4) (2015) 336–384, https://doi.org/10.1080/10643389.2013.866531.
[16] K. Dox, T. Martin, S. Houot, R. Merckx, E. Smolders, Superior residual fertiliser value in soil with phosphorus recycled from urine in layered double hydroxides, Sci. Rep. 12 (1) (2022) 8092, https://doi.org/10.1038/s41598-022-11892-4.
[17] A. Drenkova-Tuhtan, K. Mandel, A. Paulus, C. Meyer, F. Hutter, C. Gellermann, G. Sextl, M. Franzreb, H. Steinmetz, Phosphate recovery from wastewater using engineered superparamagnetic particles modified with layered double hydroxide ion exchangers, Water Res 47 (15) (2013) 5670–5677, https://doi.org/10.1016/j.watres.2013.06.039.

[18] A. Drenkova-Tuhtan, M. Schneider, M. Franzreb, C. Meyer, C. Gellermann, G. Sextl, K. Mandel, H. Steinmetz, Pilot-scale removal and recovery of dissolved phosphate from secondary wastewater effluents with reusable ZnFeZr adsorbent @ Fe3O4/SiO2 particles with magnetic harvesting, Water Res 109 (2017) 77–87, https://doi.org/10.1016/j.watres.2016.11.039.

[19] A. Drenkova-Tuhtan, M. Schneider, K. Mandel, C. Meyer, C. Gellermann, G. Sextl, H. Steinmetz, Influence of cation building blocks of metal hydroxide precipitates on their adsorption and desorption capacity for phosphate in wastewater-a screening study, Colloids Surf., A 488 (2016) 145–153, https://doi.org/10.1016/j.colsurfa.2015.10.017.

[20] A. Drenkova-Tuhtan, E.K. Sheeleigh, E. Rott, C. Meyer, D.L. Sedlak, Sorption of recalcitrant phosphonates in reverse osmosis concentrates and wastewater effluents - influence of metal ions, Water Sci. Technol. 83 (4) (2021) 934–947, https://doi.org/10.2166/wst.2021.026.

[21] M. Everaert, R. Warrinnier, S. Baken, J.P. Gustafsson, D. De Vos, E. Smolders, Phosphate-exchanged Mg-Al layered double hydroxides: a new slow release phosphate fertilizer, ACS Sustain. Chem. Eng. 4 (8) (2016) 4280–4287, https://doi.org/10.1021/acssuschemeng.6b00778.

[22] R.K. Gautam, A.K. Singh, I. Tiwari, Nanoscale layered double hydroxide modified hybrid nanomaterials for wastewater treatment: a review, J. Mol. Liq. 350 (2022), 118505, https://doi.org/10.1016/j.molliq.2022.118505.

[23] S. Goldberg, Application of surface complexation models to anion adsorption by natural materials, Environ. Toxicol. Chem. 33 (10) (2014) 2172–2180, https://doi.org/10.1002/etc.2566.

[24] X.J. Guo, Q.F. Cheng, T. Zhou, M. Xie, J. He, J.S. Guo, Y. Huang, Recovery of phosphorus from aqueous solution by iron-aluminum-zirconium-modified anthracite: performance and mechanism, ACS Sustain. Chem. Eng. 8 (23) (2020) 8577–8584, https://doi.org/10.1021/acssuschemeng.0c00956.

[25] A. Halajnia, S. Oustan, N. Najafi, A.R. Khataee, A. Lakzian, Adsorption-desorption characteristics of nitrate, phosphate and sulfate on Mg-Al layered double hydroxide, Appl. Clay Sci. 80–81 (2013) 305–312, https://doi.org/10.1016/j.clay.2013.05.002.

[26] L.C. Hsu, Y.M. Tzou, P.N. Chiang, W.M. Fu, M.K. Wang, H.Y. Teah, Y.T. Liu, Adsorption mechanisms of chromate and phosphate on hydrotalcite: a combination of macroscopic and spectroscopic studies, Environ. Pollut. 247 (2019) 180–187, https://doi.org/10.1016/j.envpol.2019.01.012.

[27] Y. Jaffer, T.A. Clark, P. Pearce, S.A. Parsons, Potential phosphorus recovery by struvite formation, Water Res 36 (7) (2002) 1834–1842, https://doi.org/10.1016/S0043-1354(01)00391-8.

[28] H.S. Ji, W.H. Wu, F.H. Li, X.X. Yu, J.J. Fu, L.Y. Jia, Enhanced adsorption of bromate from aqueous solutions on ordered mesoporous Mg-Al layered double hydroxides (LDHs), J. Hazard. Mater. 334 (2017) 212–222, https://doi.org/10.1016/j.jhazmat.2017.04.014.

[29] A.R. Jupp, S. Beijer, G.C. Narain, W. Schipper, J.C. Slootweg, Phosphorus recovery and recycling - closing the loop, Chem. Soc. Rev. 50 (1) (2021) 87–101, https://doi.org/10.1039/d0cs01150a.

[30] P. Koilraj, S. Kannan, Phosphate uptake behavior of ZnAlZr ternary layered double hydroxides through surface precipitation, J. Colloid Interface Sci. 341 (2) (2010) 289–297, https://doi.org/10.1016/j.jcis.2009.09.059.

[31] L.C. Kong, Y. Tian, Y. Wang, N. Li, Y. Liu, Z. Pang, X.H. Huang, M. Li, J. Zhang, W. Zuo, Periclase-induced generation of flowerlike clay-based layered double hydroxides: a highly efficient phosphate scavenger and solid-phase fertilizer, Chem. Eng. J. 359 (2019) 902–913, https://doi.org/10.1016/j.cej.2018.11.007.

[32] A. Kunhikrishnan, M.A. Rahman, D. Lamb, N.S. Bolan, S. Saggar, A. Surapaneni, C. R. Chen, Rare earth elements (REE) for the removal and recovery of phosphorus: a review, Chemosphere 286 (2022), 131661, https://doi.org/10.1016/j.chemosphere.2021.131661.

[33] Y.T. Lai, Y.S. Huang, C.H. Chen, Y.C. Lin, H.T. Jeng, M.C. Chang, L.J. Chen, C. Y. Lee, P.C. Hsu, N.H. Tai, Green treatment of phosphate from wastewater using a porous bio-templated graphene oxide/mgmn-layered double hydroxide composite, iScience 23 (5) (2020), 101065, https://doi.org/10.1016/j.isci.2020.101065.

[34] K.S. Le Corre, E. Valsami-Jones, P. Hobbs, S.A. Parsons, Phosphorus recovery from wastewater by struvite crystallization: a review, Crit. Rev. Environ. Sci. Technol. 39 (6) (2009) 433–477, https://doi.org/10.1080/10643380701640573.

[35] F.H. Li, J. Jin, Z.Y. Shen, H.S. Ji, M. Yang, Y.M. Yin, Removal and recovery of phosphate and fluoride from water with reusable mesoporous Fe3O4@mSiO2@mLDH composites as sorbents, J. Hazard. Mater. 388 (2020), 121734, https://doi.org/10.1016/j.jhazmat.2019.121734.

[36] F.H. Li, W.H. Wu, R.Y. Li, X.R. Fu, Adsorption of phosphate by acid-modified fly ash and palygorskite in aqueous solution: Experimental and modeling, Appl. Clay Sci. 132 (2016) 343–352, https://doi.org/10.1016/j.clay.2016.06.028.

[37] Z.G. Lin, J. Chen, Magnetic Fe3O4@MgAl-LDH@La(OH)(3) composites with a hierarchical core-shell structure for phosphate removal from wastewater and inhibition of labile sedimentary phosphorus release, Chemosphere 264 (2021), 128551, https://doi.org/10.1016/j.chemosphere.2020.128551.

[38] C. Liu, M.Y. Zhang, G. Pan, L. Lundehoj, U.G. Nielsen, Y. Shi, H.C.B. Hansen, Phosphate capture by ultrathin MgAl layered double hydroxide nanoparticles, Appl. Clay Sci. 177 (2019) 82–90, https://doi.org/10.1016/j.clay.2019.04.019.

[39] Y.H. Liu, S. Kumar, J.H. Kwag, C.S. Ra, Magnesium ammonium phosphate formation, recovery and its application as valuable resources: a review, J. Chem. Technol. Biotechnol. 88 (2) (2013) 181–189.

[40] P. Loganathan, S. Vigneswaran, J. Kandasamy, N.S. Bolan, Removal and recovery of phosphate from water using sorption, Crit. Rev. Environ. Sci. Technol. 44 (8) (2014) 847–907, https://doi.org/10.1080/10643389.2012.741311.

[41] C.Y. Lu, T.H. Kim, J. Bendix, M. Abdelmoula, C. Ruby, U.G. Nielsen, H.C.B. Hansen, Stability of magnetic LDH composites used for phosphate recovery, J. Colloid Interface Sci. 580 (2020) 660–668, https://doi.org/10.1016/j.jcis.2020.07.020.

[42] L. Lundehoj, H.C. Jensen, L. Wybrandt, U.G. Nielsen, M.L. Christensen, C.A. Quist-Jensen, Layered double hydroxides for phosphorus recovery from acidified and non-acidified dewatered sludge, Water Res 153 (2019) 208–216, https://doi.org/10.1016/j.watres.2019.01.004.

[43] K. Mandel, A. Drenkova-Tuhtan, F. Hutter, C. Gellermann, H. Steinmetz, G. Sextl, Layered double hydroxide ion exchangers on superparamagnetic microparticles for recovery of phosphate from waste water, J. Mater. Chem. A 1 (5) (2013) 1840–1848, https://doi.org/10.1039/c2ta00571a.

[44] B.K. Mayer, L.A. Baker, T.H. Boyer, P. Drechsel, M. Gifford, M.A. Hanjra, P. Parameswaran, J. Stoltzfus, P. Westerhoff, B.E. Rittmann, Total Value of Phosphorus Recovery, Environ. Sci. Technol. 50 (13) (2016) 6606–6620, https://doi.org/10.1021/acs.est.6b01239.

[45] M.B. McBride, A critique of diffuse double layer models applied to colloid and surface chemistry, Clays Clay Min. 45 (4) (1997) 598–608, https://doi.org/10.1346/Ccmn.1997.0450412.

[46] M.C. Monea, C. Meyer, H. Steinmetz, H. Schonberger, A. Drenkova-Tuhtan, Phosphorus recovery from sewage sludge - phosphorus leaching behavior from aluminum-containing tertiary and anaerobically digested sludge, Water Sci. Technol. 82 (8) (2020) 1509–1522, https://doi.org/10.2166/wst.2020.414.

[47] K. Morimoto, S. Anraku, J. Hoshino, T. Yoneda, T. Sato, Surface complexation reactions of inorganic anions on hydrotalcite-like compounds, J. Colloid Interface Sci. 384 (2012) 99–104, https://doi.org/10.1016/j.jcis.2012.06.072.

[48] G.K. Morse, S.W. Brett, J.A. Guy, J.N. Lester, Review: phosphorus removal and recovery technologies, Sci. Total Environ. 212 (1) (1998) 69–81, https://doi.org/10.1016/S0048-9697(97)00332-X.

[49] G.Z. Nie, L.R. Wu, S.J. Qiu, Z.W. Xu, H.L. Wang, Preferable phosphate sequestration using polymer-supported Mg/Al layered double hydroxide nanosheets, J. Colloid Interface Sci. 614 (2022) 583–592, https://doi.org/10.1016/j.jcis.2022.01.158.

[50] F. Ogata, N. Nagai, M. Kishida, T. Nakamura, N. Kawasaki, Interaction between phosphate ions and Fe-Mg type hydrotalcite for purification of wastewater, J. Environ. Chem. Eng. 7 (2019), 102897, https://doi.org/10.1016/j.jece.2019.102897.

[51] Olympus, DELTA Family Handheld XRF Analyzer: User's Manual, International ed, Waltham, MA, USA, 2013.

[52] K.Y. Park, J.H. Song, S.H. Lee, H.S. Kim, Utilization of a selective adsorbent for phosphorus removal from wastewaters, Environ. Eng. Sci. 27 (9) (2010) 805–810, https://doi.org/10.1089/ees.2010.0139.

[53] W.C. Qiao, H. Bai, T.H. Tang, J.H. Miao, Q.W. Yang, Recovery and utilization of phosphorus in wastewater by magnetic Fe3O4/Zn-Al-Fe-La layered double hydroxides(LDHs), Colloids Surf., A 577 (2019) 118–128, https://doi.org/10.1016/j.colsurfa.2019.05.046.

[54] M. Ramachandran, R. Subadevi, W.-R. Liu, M. Sivakumar, Facile synthesis and characterization of ZrO2 nanoparticles via modified Co-precipitation method, J. Nanosci. Nanotechnol. 18 (1) (2018) 368–373, https://doi.org/10.1166/jnn.2018.14562.

[55] B.E. Rittmann, B. Mayer, P. Westerhoff, M. Edwards, Capturing the lost phosphorus, Chemosphere 84 (6) (2011) 846–853, https://doi.org/10.1016/j.chemosphere.2011.02.001.

[56] M. Schneider, A. Drenkova-Tuhtan, W. Szczerba, C. Gellermann, C. Meyer, H. Steinmetz, K. Mandel, G. Sextl, Nanostructured ZnFeZr oxyhydroxide precipitate as efficient phosphate adsorber in waste water: understanding the role of different material-building-blocks, Environ. Sci. - Nano 4 (1) (2017) 180–190, https://doi.org/10.1039/c6en00507a.

[57] Sparks, D.L., 2003. 5 - Sorption Phenomena on Soils, in: Sparks, D.L. (Ed.) Environmental Soil Chemistry (Second Edition). Academic Press, Burlington, pp. 133–186. https://doi.org/10.1016/B978–012656446-4/50005–0.

[58] V. Stefov, B. Soptrajanov, I. Kuzmanovski, H.D. Lutz, B. Engelen, Infrared and Raman spectra of magnesium ammonium phosphate hexahydrate (struvite) and its isomorphous analogues. III. Spectra of protiated and partially deuterated magnesium ammonium phosphate hexahydrate, J. Mol. Struct. 752 (1–3) (2005) 60–67, https://doi.org/10.1016/j.molstruc.2005.05.040.

[59] K.S. Triantafyllidis, E.N. Peleka, V.G. Komvokis, P.P. Mavros, Iron-modified hydrotalcite-like materials as highly efficient phosphate sorbents, J. Colloid Interface Sci. 342 (2) (2010) 427–436, https://doi.org/10.1016/j.jcis.2009.10.063.

[60] B.L. Wu, J. Wan, Y.Y. Zhang, B.C. Pan, I.M.C. Lo, Selective phosphate removal from water and wastewater using sorption: process fundamentals and removal mechanisms, Environ. Sci. Technol. 54 (1) (2020) 50–66, https://doi.org/10.1021/acs.est.9b05569.

[61] Y. Xu, T.J. Liu, Y.K. Huang, J.Y. Zhu, R.L. Zhu, Role of phosphate concentration in control for phosphate removal and recovery by layered double hydroxides, Environ. Sci. Pollut. R. 27 (14) (2020) 16612–16623, https://doi.org/10.1007/s11356-020-08102-x.

[62] H.L. Yan, Q.W. Chen, J.H. Liu, Y. Feng, K.M. Shih, Phosphorus recovery through adsorption by layered double hydroxide nano-composites and transfer into a struvite-like fertilizer, Water Res 145 (2018) 721–730, https://doi.org/10.1016/j.watres.2018.09.005.

[63] J.N. Yan, M.Y. Ma, K.Y. Liu, Y. Bao, F.H. Li, Anchoring NH2-MIL-101(Fe/Ce) within melamine sponge boosts rapid adsorption and recovery of phosphate from water, ACS EST Eng. 3 (4) (2023) 467–478, https://doi.org/10.1021/acsestengg.2c00324.

[64] F. Yang, S.S. Zhang, Y.Q. Sun, D.C.W. Tsang, K. Cheng, Y.S. Ok, Assembling biochar with various layered double hydroxides for enhancement of phosphorus recovery, J. Hazard. Mater. 365 (2019) 665–673, https://doi.org/10.1016/j.jhazmat.2018.11.047.

[65] R.T. Yu, J.J. Geng, H.Q. Ren, Y.R. Wang, K. Xu, Struvite pyrolysate recycling combined with dry pyrolysis for ammonium removal from wastewater, Bioresour. Technol. 132 (2013) 154–159, https://doi.org/10.1016/j.biortech.2013.01.015.

[66] Q. Zhang, F.Y. Ji, T.T. Zhao, Q.S. Shen, D.X. Fang, L. Kuang, L. Jiang, S.L. Ding, Systematic screening of layered double hydroxides for phosphate removal and mechanism insight, Appl. Clay Sci. 174 (2019) 159–169, https://doi.org/10.1016/j.clay.2019.03.030.

[67] Y.Y. Zhang, B. Kong, Z.Y. Shen, J.S. Qian, B.C. Pan, Phosphorus binding by lanthanum modified pyroaurite-like clay: performance and mechanisms, ACS EST Eng. 1 (11) (2021) 1565–1575, https://doi.org/10.1021/acsestengg.1c00218.